energies

MDPI

Article

Effect of Morphological Characteristics of Aggregates on Thermal Properties of Molten Salt Nanofluids

Weichao Zhang [1], Chaoyang Zhu [1], Shuanjun Chen [1], Shixing Wang [1], Zhaoshuo Jing [2,3] and Liu Cui [2,3,*]

[1] State Grid Energy Hefeng Coal Power Co., Ltd., Tacheng 834700, China
[2] State Key Laboratory of Alternate Electrical Power System with Renewable Energy Sources, North China Electric Power University, Beijing 102206, China
[3] Key Laboratory of Power Station Energy Transfer Conversion and System, North China Electric Power University, Ministry of Education, Beijing 102206, China
* Correspondence: liucui@ncepu.edu.cn; Tel.: +86-010-61773958

Abstract: Molten salt-based nanofluid is a thermal storage and heat transfer medium for concentrated solar thermal power plants formed by adding nanoparticles to molten salt, which can enhance the thermal performance of molten salt. However, the nanoparticles tend to aggregate in nanofluids, causing changes in thermal properties. In this work, molecular dynamics simulations were used to study the effect of morphological characteristics of aggregates on the thermal conductivity and specific heat capacity of molten salt-based nanofluids. The results show that the aggregated nanoparticles cause a greater increase in thermal conductivity and specific heat capacity than dispersed nanoparticles. Additionally, the increase in fractal dimension leads to thermal conductivity reduction, while there is no clear correlation between the fractal dimension and specific heat capacity. New insights into the thermal properties of aggregated nanofluids are provided by analyzing the contribution of material components, heat flux fluctuation modes, and energy compositions. It is found that the thermal conductivity of aggregated nanofluids is mainly dominated by the base liquid and collision term. However, the specific heat is not related to the variation in the contribution of different energy compositions. Moreover, compared to the dispersed nanofluid, the increased specific heat capacity of aggregated nanofluids is attributed to the thicker semi-solid layer. This study provides guidance for the design and control of the thermal properties of molten salt-based nanofluids.

Keywords: nanofluids; solar salt; molecular dynamics; agglomerate; fractal dimension

check for updates

Citation: Zhang, W.; Zhu, C.; Chen, S.; Wang, S.; Jing, Z.; Cui, L. Effect of Morphological Characteristics of Aggregates on Thermal Properties of Molten Salt Nanofluids. *Energies* **2024**, *17*, 1080. https://doi.org/10.3390/en17051080

Academic Editor: Christopher Micallef

Received: 28 December 2023
Revised: 23 January 2024
Accepted: 13 February 2024
Published: 24 February 2024

Copyright: © 2024 by the authors. Licensee MDPI, Basel, Switzerland. This article is an open access article distributed under the terms and conditions of the Creative Commons Attribution (CC BY) license (https://creativecommons.org/licenses/by/4.0/).

1. Introduction

Solar energy is abundant and emits very few pollutants, making it an important energy source to alleviate energy problems [1]. Concentrated solar thermal power (CSP) is a promising solar energy technology. Thermal energy storage (TES) is a necessary part of a CSP plant, where stored heat can be used for continuous operation of the CSP plant during the night and on cloudy days [2] and, thus, help to improve power supply quality [3]. Molten salts are widely used as the thermal storage material and heat transfer medium in CSP systems due to their high latent heat, low vapor pressure, wide operating temperature range, and low cost [4]. However, the low thermal conductivity of molten salts reduces the charge–discharge rate and decreases the efficiency of TES systems. The low specific heat capacity leads to problems such as the larger scale of the heat storage system and the greater consumption of heat storage materials. These increase the cost and reduce the economy of CSP systems [5,6].

Numerous studies have shown that the addition of nanoparticles can enhance the thermal performance of molten salts [7–15]. However, nanoparticles in molten salt-based nanofluids tend to aggregate and settle easily [16–18], affecting the thermal performance of nanofluids. Only a few studies have focused on the effect of nanoparticle aggregation on thermal conductivity. In addition, the effect of aggregation on specific heat capacity is often

overlooked. It has been found that nanoadditive aggregation could promote heat conduction in water containing metal oxide nanoparticles and carbon nanotubes [19]. Similarly enhanced thermal conductivity has been reported for Fe_3O_4–water nanofluids. When the aggregates are properly oriented, and the volume fraction of aggregates accounts for 65% of the total nanoparticle, the enhancement of thermal conductivity is the highest [20]. The enhancement in thermal conductivity is attributed to the formation of the heat conduction pathways, which are formed by aggregates and have low thermal resistance [7,21]. In contrast, the research of Al_2O_3–water nanofluids [11], ZnO–propylene glycol nanofluids [10], and CuO–water as well as CuO–ethylene glycol nanofluids [9] found that aggregation limited the thermal conductivity of nanofluids. This may be attributed to the reduction in the specific surface area of nanoparticles, limiting the effective area of thermal interaction between the base liquid and nanoparticles. To date, the impact of aggregation on the thermal conductivity of nanofluids remains a controversial issue.

On the other hand, different morphological characteristics of aggregates, such as fractal dimension, size, and shape, have an influence on the thermal properties of aggregated nanofluids [22]. The nanoparticle agglomerates can be characterized by fractal dimension, which represents the tightness of nanoparticle aggregation. The effect of the fractal dimension of nanoparticles on the specific heat capacity has been rarely studied, and only a few articles have investigated the fractal dimension's influence on thermal conductivity. Wang et al. [23] studied Cu–Ar nanofluid through molecular dynamics simulation and found that the lower the fractal dimension of the nanoparticle, the greater the thermal conductivity. Li et al. [24] and Du et al. [25] also found the same conclusion in Cu–water nanofluid. The low fractal dimension is more likely to produce effective heat channels and, hence, promotes the heat transfer process inside the aggregated nanofluids [23,24]. However, all of the previous research concerns molecular liquids, such as Cu–Ar and Cu–water nanofluids. Whether the same conclusion can be drawn about ionic liquids, such as solar salt-based nanofluids, remains to be explored. Additionally, the underlying mechanism of the effect of agglomeration morphology on thermophysical properties is still unclear and needs to be studied further.

Solar salt ($NaNO_3$:KNO_3 = 60:40 wt.%) is the most-used working fluid in CSP systems due to its low melting point and, thus, a large liquid phase range, resulting in a large operating range and minimal energy demand to remain in liquid form [26]. Therefore, it was selected as the base fluid in this work. In addition, SiO_2 nanoparticles, which have the advantages of easy fabrication, low cost, and chemical stability in solar salt, were selected as the additive. To explore the impact of the fractal dimension of aggregates on the thermal properties of nanofluids and reveal its mechanism, the thermal conductivity and specific heat capacity of SiO_2–solar salt were calculated using molecular dynamics (MD) simulations. The deeper heat conduction and thermal energy storage mechanisms were obtained from the semi-solid layer, the contributions of different material components and heat flux fluctuation modes to thermal conductivity, and the contributions of different energy compositions to specific heat capacity.

2. Simulation Model and Method

The model of solar salt is shown in Figure 1a. Following the density of solar salt ($NaNO_3$:KNO_3 = 60:40 wt.%) of 1.9 g/cm^3 [27], Na^+, K^+, and NO_3^- ions were randomly filled in a cubic box with a side length of 55 Å, which is large enough to avoid the finite size effect [28]. Due to the limitations of computer resources, four spherical SiO_2 nanoparticles with a diameter of 18 Å were created, as shown in Figure 1b. Nanoparticle diameters around 2 nm have been used in previous MD simulations [29,30]. The nanoparticles were randomly filled in the solar salt box to obtain a dispersed nanofluid, as shown in Figure 1c. Then, nanoparticle aggregates with different fractal dimensions were created. Figure 1d–g shows

aggregated nanofluids under 8 wt.% loading of nanoparticles. The fractal dimension (D_f) represents the tightness of nanoparticle aggregation, which is given by Equation (1) [23].

$$N_P = (\frac{R_g}{R})^{D_f} \quad (1)$$

Here, N_P is the number of primary nanoparticles of radius R, and R_g is the radius of gyration.

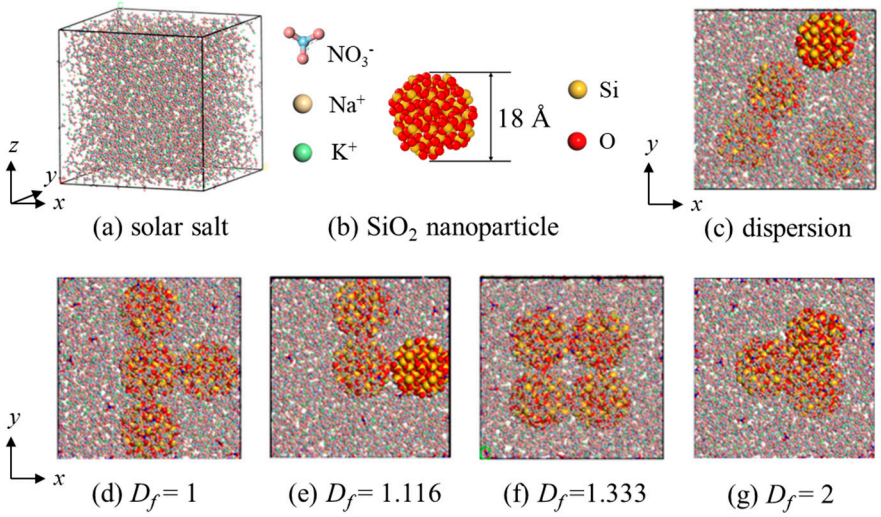

Figure 1. Models of (**a**) solar salt, (**b**) SiO_2 nanoparticle, (**c**) dispersed nanofluid, and (**d**–**g**) aggregated nanofluids.

All MD simulations were done with the open-source LAMMPS (Large-scale Atomic/Molecular Massively Parallel Simulator, 2020OCT29) package [31]. The time step was set to 0.5 fs, and periodic boundary conditions were applied in all three dimensions. The Buckingham potential [32] was employed to describe the interactions between ions in nitrate salts, the interactions among atoms within SiO_2 nanoparticles, and the interactions between SiO_2 nanoparticle atoms and nitrate salt ions [33]. The Buckingham potential is expressed by Equation (2) [32].

$$E = A_{ij} e^{-\frac{r_{ij}}{\rho_{ij}}} - \frac{C_{ij}}{r_{ij}^6} + \frac{q_i q_j}{r_{ij}} \quad (2)$$

Here, i and j represent different atoms, respectively. r_{ij} represents the distance between atoms i and j. q_i and q_j represent the number of charges of atoms i and j, respectively. ρ_{ij} is an ionic-pair-dependent length parameter, and the coefficients A_{ij} and C_{ij} are two potential parameters related to energy. The parameters of the various atoms in Equation (2) are shown in Table 1.

Table 1. Parameters of Buckingham potential function [29].

Atom	q_i/e	A_{ii}/Kcal·mol^{-1}	ρ_{ii}/Å	C_{ii}/Kcal·mol^{-1}·Å^6
N	0.95	33,652.75	0.2646	259.1
Na	1	9778.06	0.3170	24.18
K	1	35,833.47	0.3370	349.9
O (In NO_3^-)	−0.65	62,142.9	0.2392	259.4
O (In SiO_2)	−0.955209	15,170.70	0.386	617.24
Si	1.910418	72,460.64	0.351	14,415.29

For the Buckingham potential function, the parameters of the interactions between the different atoms were calculated by the Lorentz–Berthelot mixing rule [32], i.e., $A_{ij} = (A_{ii} A_{jj})^{1/2}$, $C_{ij} = (C_{ii} C_{jj})^{1/2}$,$1/\rho_{ij} = (1/\rho_{ii} + 1/\rho_{jj})/2$.

In nitrate, the bonded interactions were described using the Harmonic potential [34] as given in Equation (3) and Charmm potential [35] as given in Equation (4).

$$E = K_r(r - r_0)^2 \tag{3}$$

$$E = K_\theta(\theta - \theta_0)^2 + K_{UB}(r - r_{UB})^2 \tag{4}$$

In Equation (3), r is the N–O bond length, r_0 is the equilibrium bond length, and K_r is the force constant. In Equation (4), the first term on the right of equal sign is the simple harmonic term for O–N–O bond angle bending, the second term on the right of equal sign is the O–O non-bonding repulsion term, θ is the O–N–O bond angle, θ_0 is the equilibrium bond angle, K_θ is the force constant, r is the O–O distance, r_{UB} is the equilibrium distance, and K_{UB} is the Urey–Bradley force constant. The parameters of Harmonic potential and Charmm potential are shown in Table 2.

Table 2. Parameters of Harmonic potential and Charmm potential [32].

Group	K_r/eV·10^{-20} m	r_0/10^{-10} m	K_θ/eV	θ_0/°	K_{UB}/eV	r_{UB}/10^{-10} m
NO_3^-	17.5344	1.2676	2.7122	120	4.9608	2.1955

The calculation of thermal conductivity adopts the equilibrium molecular dynamics (EMD) method. For solar salts in the CSP plant, the working temperature range is 563–861 K [36] at ambient pressure of 1 bar [37]. In order to obtain an equilibrium state, the systems were equilibrated in an NPT ensemble for 0.5 ns, with a pressure of 1 bar and temperature of 573.15 K, and then under the NVT ensemble for 1 ns, followed by a final 2 ns simulation in the NVE ensemble. After that, the thermal conductivity was obtained in the NVE ensemble for another 0.5 ns. The thermal conductivity was obtained through the heat current autocorrelation function (HCACF) using the Green–Kubo formula [38], as shown in Equation (5).

$$\lambda(t) = \frac{V}{k_B T^2} \int_0^t < J(0)J(t) > dt \tag{5}$$

Here, k_B, V, and T are Boltzmann constants, the system volume and temperature, respectively. $<J(0)J(t)>$ is the ensemble average of HCACF. $J(t)$ denotes the heat flux of the system at the time t [39], and its expression is shown in Equation (6).

$$\boldsymbol{J} = \frac{1}{V}\sum_i \left[(E_{k,i} + E_{p,i} - \langle h_i \rangle)\boldsymbol{v}_i + \sum_{j,j\neq i} \left(\boldsymbol{f}_{ij} \cdot \boldsymbol{r}_{ij} \right) \boldsymbol{v}_j \right] \tag{6}$$

Here, $\boldsymbol{v}_i$ and E_i represent the velocity vector and total energy of atom i, respectively. $\boldsymbol{r}_{ij}$ and $\boldsymbol{f}_{ij}$ represent the distance and interaction force between atoms i and j, respectively. N denotes the total number of atoms in the system. It is worth noting that in Equation (6), the third term on the right of the equal sign represents the partial enthalpy. For a single-component system, the partial enthalpy is 0. However, for a multi-component system such as solar salt-based nanofluids, the partial enthalpy is non-zero. This portion of heat flux does not contribute to thermal conductivity and needs to be subtracted [39].

The calculation of specific heat capacity adopts the energy fluctuation method. In order to obtain an equilibrium state, the systems were equilibrated in the NPT ensemble for 0.5 ns, with the pressure of 1 bar and temperature of 573.15 K, and then under the

NVT ensemble for 1 ns. After that, the specific heat capacity C was obtained in the NVT ensemble for another 1 ns. The C is calculated as Equations (7) and (8) [40].

$$C = \frac{\sigma_E^2}{mk_B T^2} \tag{7}$$

$$\sigma_E^2 = < E^2 > - < E >^2 \tag{8}$$

Here, σ_E^2 denotes the rise and fall of the total energy of the system under the NVT ensemble. <> represents the average value of the system with the number of atoms as the weight, and m is the atom mass.

3. Results and Discussion

3.1. Thermal Conductivity and Specific Heat Capacity

Figure 2a shows the thermal conductivity of solar salt and nanofluids. The obtained thermal conductivity of solar salt at 573.15 K is 0.487 $W \cdot m^{-1} \cdot K^{-1}$, which is similar to the experimental results of 0.500 $W \cdot m^{-1} \cdot K^{-1}$ [41]. It validates the reliability of the potential energy functions and simulation method chosen in this study. It can also be observed from Figure 2a that the addition of nanoparticles leads to an increase in thermal conductivity. A similar result has been reported for binary nitrate salt with SiO_2 nanoparticles in experiments [42]. Moreover, compared with the dispersed nanoparticles, the addition of aggregated nanoparticles results in a higher thermal conductivity. This result is different from that observed in previous experiments [43–45]. Nasiri et al. [43] and Kazemi et al. [44] found that the thermal conductivity of nanofluids with small agglomeration and low settling is larger than that of nanofluids with large agglomeration and high settling. The contradictory conclusions between simulations and experiments are attributed to different stabilities, i.e., no settling and high settling. As the nanoparticle aggregates settle, the concentration of nanoparticles in the system decreases; that is, the mass fraction of the nanofluid decreases, resulting in a decrease in thermal conductivity [46]. However, in MD simulations, there is no sedimentation in aggregated nanofluids. Figure 2a also shows that the smaller the fractal dimension of the aggregates, the higher the thermal conductivity of the nanofluid. As the fractal dimension increases from 1 to 2, the thermal conductivity decreases by 14.15%. Similar results have been reported in Cu/water nanofluid [24] and Cu/Ar nanofluid [23].

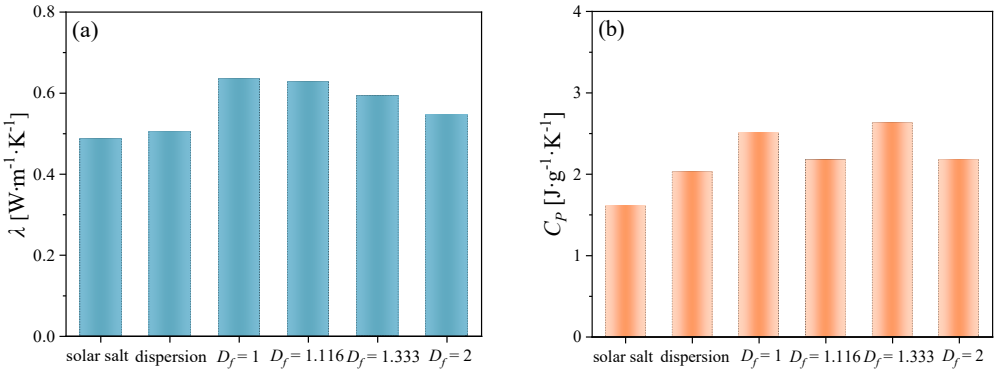

Figure 2. (**a**) Thermal conductivity and (**b**) specific heat of solar salt and nanofluids at 573.15 K.

Figure 2b shows the specific heat capacities of solar salt, dispersed nanofluid, and aggregated nanofluids with different fractal dimensions at 573.15 K. The specific heat capacity of solar salt at 573.15 K is determined to be 1.610 $J \cdot g^{-1} \cdot K^{-1}$, which is close to the experimental value of 1.648 $J \cdot g^{-1} \cdot K^{-1}$ obtained in the literature [47]. As shown in Figure 2b, the specific heat capacity of nanofluids is increased compared to solar salt, whether adding agglomerated or dispersed nanoparticles. However, the fractal dimension of nanoparticle

aggregates is not directly related to the specific heat capacity, which is different from the monotonous dependence of thermal conductivity on the fractal dimension.

3.2. Contributions of Different Material Components and Heat Flux Fluctuation Modes to Thermal Conductivity

In order to study the heat conduction mechanism of aggregate nanofluids, the contributions of nanoparticles and base liquid to the thermal conductivity were examined, respectively. The heat flux of nanoparticle $\boldsymbol{J}_{\mathrm{N}}$ and base liquid $\boldsymbol{J}_{\mathrm{B}}$ is shown in Equations (9) and (10) [48]. Hence, according to the Green–Kubo formula, the thermal conductivity can be calculated as a sum of four terms, including the self-correlations (i.e., λ_{BB} and λ_{NN}) and crossed correlations (including λ_{BN} and λ_{NB}).

$$\boldsymbol{J}_{\mathrm{N}}(t) = \frac{1}{V}\sum_{i,i\in \mathrm{N}}\left[\left(E_{k,i} + E_{p,i} - \langle h_i\rangle\right)\boldsymbol{v}_i + \sum_{j,j\neq i}\left(\boldsymbol{f}_{ij}\cdot\boldsymbol{r}_{ij}\right)\boldsymbol{v}_j\right] \tag{9}$$

$$\boldsymbol{J}_{\mathrm{B}}(t) = \frac{1}{V}\sum_{i,i\in \mathrm{N}}\left[\left(E_{k,i} + E_{p,i} - \langle h_i\rangle\right)\boldsymbol{v}_i + \sum_{j,j\neq i}\left(\boldsymbol{f}_{ij}\cdot\boldsymbol{r}_{ij}\right)\boldsymbol{v}_j\right] \tag{10}$$

It is found that the contributions of crossed correlations are small, which has also been reported in Cu–Ar nanofluid [49]. Therefore, Figure 3a only shows the contributions of nanoparticles and base liquid to thermal conductivity due to self-correlations. It can be seen that the contribution of base fluid is about 70%, which is much larger than aggregated nanoparticles. In addition, the contribution of base fluid decreases with the increase of fractal dimension. As the fractal dimension increases from 1.116 to 2, the contribution of λ_{BB} decreases by 6.95%. This tendency is consistent with the thermal conductivity shown in Figure 2a. It indicates that the base liquid dominates the heat conduction of aggregated nanofluids.

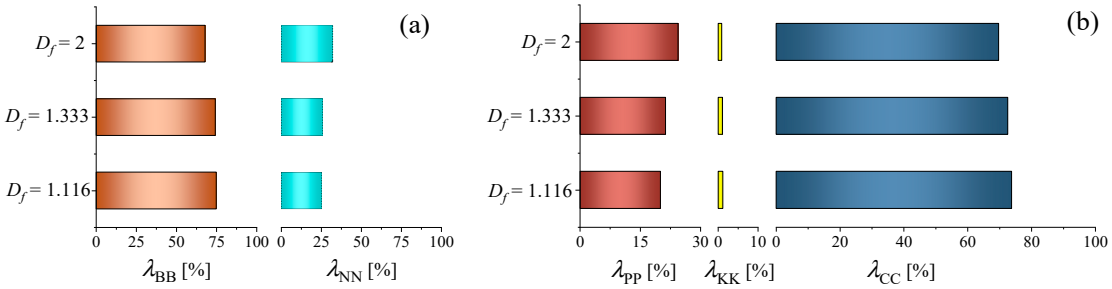

Figure 3. (**a**) Contributions of base fluid and nanoparticle to thermal conductivity. (**b**) Contributions of kinetic, potential, and collision terms to thermal conductivity.

On the other hand, the heat flux vector can be decomposed into three terms (i.e., the kinetic (K), potential (P), and collision (C) terms), as shown in Equations (11) and (12) [50]. Therefore, the thermal conductivity can be calculated as a sum of nine terms, including self-correlations (i.e., λ_{KK}, λ_{PP}, and λ_{CC}) and crossed correlations (including λ_{PC}, λ_{CP}, λ_{PK}, λ_{KP}, λ_{KC}, and λ_{CK}).

$$J = \sum_{k=\alpha}^{\beta}\sum_{l}^{N_k}\underbrace{\frac{1}{2}m_{ix}^{k}\left(v_{ix}^{k}\right)^2}_{\mathrm{K}}v_i^k + \sum_{k=\alpha}^{\beta}\sum_{l=\alpha}^{\beta}\sum_{i=l}^{N_k}\sum_{j>i}^{N_l}\left[\underbrace{IU\left(r_{ij}^{kl}\right)}_{\mathrm{P}} - \underbrace{r_{ij}^{kl}\otimes\frac{\partial U\left(r_{ij}^{kl}\right)}{\partial r_{ij}^{kl}}}_{\mathrm{C}}\right]\cdot v_i^k - \sum_{k=\alpha}^{\beta}h^k\sum_{i=l}^{N_k}h^k v_i^k \tag{11}$$

$$U(\mathbf{r}_{ij}^{kl}) = A\left(1 - \frac{r_{ij}}{r_c}\right)^2 \tag{12}$$

Here, α and β represent solar salt and SiO_2 nanoparticles. k and l represent different components. m_i and v_i are the mass and velocity of atom i, and h is the mean partial enthalpy. A is an arbitrary constant, and r_c is the cutoff radius.

The results show that the contributions of crossed correlations are negligible, which is consistent with that reported in Pt/Xe nanofluid [50]. Hence, the contributions due to self-correlations are given in Figure 3b. As can be seen, the contribution of λ_{KK} is small, which means Brownian motion has minimal effect on thermal conductivity. Similar results have been found in dispersed nanofluids [30]. Moreover, the enhancement in thermal conductivity of aggregated nanofluids is primarily dominated by λ_{CC}, which is larger than 60%. The fractal dimension of aggregates shows a negative correlation with λ_{CC}. As the fractal dimension increases from 1.116 to 2, the contribution of λ_{CC} decreases by 5.55%. This trend is the same with the thermal conductivity shown in Figure 2a. It suggests that the collision term may be responsible for the reduced thermal conductivity of nanofluids with larger fractal dimensions.

3.3. Contributions of Different Energy Compositions to Specific Heat Capacity

To reveal the physical insights of specific heat capacity, the effects of different energy components on the specific heat capacity of the nanofluid were explored. The contributions of kinetic and potential energy to the specific heat capacity were calculated first. The results are shown in Figure 4a. We can see that the contribution of potential energy is larger than that of kinetic energy. We further decomposed the contribution of potential energy to the van der Waals C_{vdwl}, short-ranged part of coulombic interaction C_{coul}, long-ranged part of coulombic interaction C_{long}, bond C_{bond}, angle $C_{angle,}$ and improper C_{impro} potentials, as shown in Figure 4b. It can be seen that the ranking of contribution is $C_{long} < C_{impro} < C_{bond} < C_{angle} < C_{vdwl} < C_{coul}$. The contribution of C_{coul} is the largest and negatively correlated with the fractal dimension. As the fractal dimension increases from 1.116 to 2, the contribution of C_{coul} decreases by 30.17%. Differently, the specific heat capacity changes with fractal dimensions are irregular. The correlation between specific heat and the variation in the contribution of different energy compositions needs to be further explored. We hope that our findings can stimulate interest in studying the relationship between the specific heat and energy composition contribution.

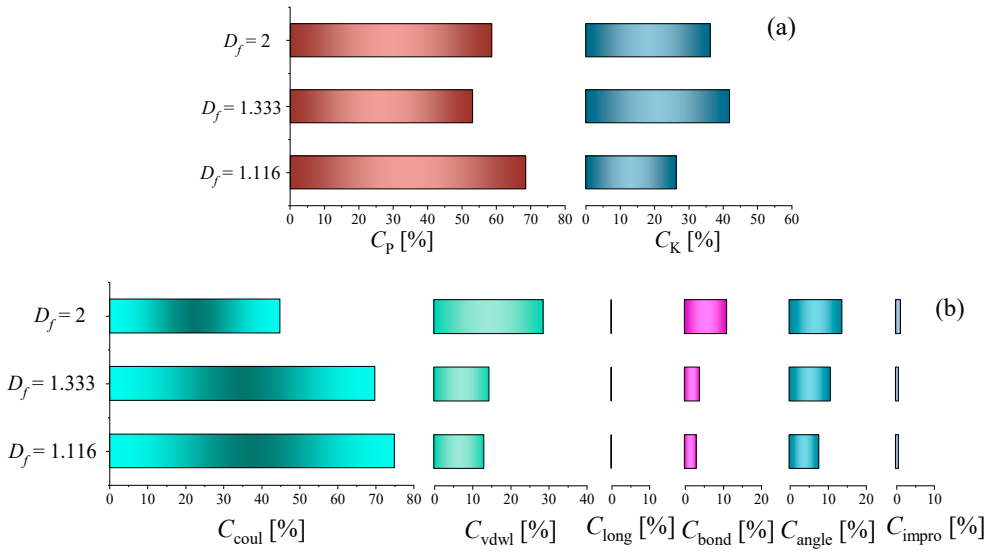

Figure 4. (**a**) Contributions of the kinetic and potential to specific heat capacity. (**b**) Contributions of the van der Waals, short-ranged part of coulombic interaction, long-ranged part of coulombic interaction, bond, angle, and improper potentials to specific heat capacity.

3.4. Semi-Solid Layer

The density distribution of ions around the nanoparticle was further calculated and is shown in Figure 5a. As can be seen, the first peak of density is the greatest, then the other peaks weaken. This indicates that the addition of nanoparticles results in a strong attraction between nanoparticles and the base liquid, leading to the formation of a semi-solid layer. Destroying the microstructure of the semi-solid layer requires energy, thus increasing the specific heat capacity of the nanofluid. The thickness of the semi-solid layer is measured from the first peak to the third trough [51] of density distribution. Figure 5b shows the thickness of the semi-solid layer around dispersed nanoparticles and aggregated nanoparticles. We can find that the thickness of the semi-solid layer around agglomerated nanoparticles is greater than that around dispersed nanoparticles. In addition, the quantitative relationship of the semi-solid layer thickness shown in Figure 5b is consistent with the specific heat shown in Figure 2b. It verifies that the semi-solid layer is related to the specific heat. However, the quantitative relationship of semi-solid layer thickness does not correspond to the thermal conductivity. This indicates that the change in heat conduction of aggregated nanofluids cannot be explained by the semi-solid layer. Similar results have been found in dispersed nanofluids [29,30].

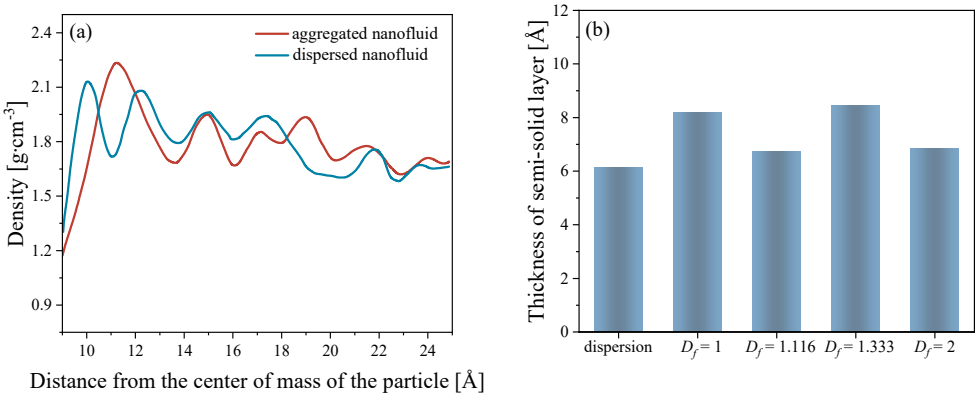

Figure 5. Density distribution of (**a**) base fluid around nanoparticles and (**b**) statistics of the thickness of semi-solid layer.

Apart from the addition of nanoparticles, the aggregate morphology can also provide a degree of freedom to promote the heat transfer and energy conversion efficiency of molten salt. Filling nanoparticles results in an increase in both specific heat capacity and thermal conductivity of molten salt, while the aggregate morphology has different effects on heat storage and heat transfer properties. Different from the irregular dependence of specific heat capacity on aggregate morphology, there is a negative correlation between aggregate morphology and thermal conductivity. Higher thermal conductivity can be obtained for a nanofluid with smaller aggregates by chemically treating the nanoparticles [52], adding surfactants [53], and changing pH values [54].

4. Conclusions

In this paper, the thermal conductivity and specific heat capacity of solar salt-based nanofluids were investigated by MD simulations. The results show that the addition of SiO_2 nanoparticles increases the thermal conductivity and specific heat capacity of solar salt, and the aggregated nanofluids have greater thermal conductivity and specific heat capacity than the dispersed ones. It is interesting to find that the aggregate morphological characteristics have different effects on the thermal conductivity and specific heat capacity of nanofluids. The thermal conductivity decreases with increasing fractal dimension, while the fractal dimension has no correlation with specific heat capacity. Based on the analysis of the contributions of different material components and heat flux fluctuation modes to thermal conductivity and contributions of different energy compositions to specific heat

capacity, new insights into heat conduction and thermal energy storage were provided. It was found that the base fluid and collision term have the dominant impact on the heat conduction of aggregated nanofluids. Moreover, the thickness of the semi-solid layer is related to specific heat capacity. This MD study is focused on the new phenomena and physical insights into the thermal properties of aggregated nanofluids on the nanoscale. It is expected that the findings can inspire others to pursue the thermal properties of aggregated nanofluids at meso and macro scales.

Author Contributions: Conceptualization, W.Z., C.Z., S.C., S.W. and Z.J.; methodology, W.Z., C.Z., S.C., S.W. and Z.J.; software, L.C.; validation, L.C.; formal analysis, L.C.; investigation, L.C.; writing—original draft preparation, L.C.; writing—review and editing, L.C.; visualization, L.C.; funding acquisition, L.C. All authors have read and agreed to the published version of the manuscript.

Funding: The authors are thankful for financial support from the National Natural Science Foundation of China (No. 52090062), the National Key R&D Program of China (2022YFB2405202), and the Fundamental Research Funds for the Central Universities (No. 2023JC001).

Data Availability Statement: Data are contained within the article.

Acknowledgments: The authors thank National Supercomputing Center in Tianjin for the support.

Conflicts of Interest: W.Z., C.Z., S.C. and S.W. were employed by State Grid Energy Hefeng Coal Power Co., Ltd. The remaining authors declare that the research was conducted in the absence of any commercial or financial relationships that could be construed as a potential conflict of interest.

References

1. Praveen, R.; Baseer, M.A.; Sankara, N.K. Design. Performance analysis and optimization of a 100 MW concentrated solar power plant with thermal energy storage. In Proceedings of the 2018 International Conference on Current Trends towards Converging Technologies (ICCTCT), Coimbatore, India, 1–3 March 2018; pp. 1–6. [CrossRef]
2. Islam, M.T.; Huda, N.; Abdullah, A.; Saidur, R. A comprehensive review of state-of-the-art concentrating solar power (CSP) technologies: Current status and research trends. *Renew. Sustain. Energy Rev.* **2018**, *91*, 987–1018. [CrossRef]
3. El Alami, K.; Asbik, M.; Agalit, H. Identification of natural rocks as storage materials in thermal energy storage (TES) system of concentrated solar power (CSP) plants—A review. *Sol. Energy Mater. Sol. Cells* **2020**, *217*, 110599. [CrossRef]
4. Rao, Z.; Bai, R.; Ye, K.; Zhou, T. Effects of interfacial layer on thermal conductivity enhancement of solar salt-based nanofluids: Insights from molecular dynamics simulations. *Case Stud. Therm. Eng.* **2022**, *35*, 102087. [CrossRef]
5. Nunes, V.; Queirós, C.; Lourenço, M.; Santos, F.; De Castro, C.N. Molten salts as engineering fluids—A review: Part I. Molten alkali nitrates. *Appl. Energy* **2016**, *183*, 603–611. [CrossRef]
6. Da Cunha, J.P.; Eames, P. Thermal energy storage for low and medium temperature applications using phase change materials—A review. *Appl. Energy* **2016**, *177*, 227–238. [CrossRef]
7. Evans, W.; Prasher, R.; Fish, J.; Meakin, P.; Phelan, P.; Keblinski, P. Effect of aggregation and interfacial thermal resistance on thermal conductivity of nanocomposites and colloidal nanofluids. *Int. J. Heat Mass Transf.* **2008**, *51*, 1431–1438. [CrossRef]
8. Wu, C.; Cho, T.J.; Xu, J.; Lee, D.; Yang, B.; Zachariah, M.R. Effect of nanoparticle clustering on the effective thermal conductivity of concentrated silica colloids. *Phys. Rev. E* **2010**, *81*, 011406. [CrossRef] [PubMed]
9. Karthikeyan, N.; Philip, J.; Raj, B. Effect of clustering on the thermal conductivity of nanofluids. *Mater. Chem. Phys.* **2008**, *109*, 50–55. [CrossRef]
10. Suganthi, K.S.; Parthasarathy, M.; Rajan, K.S. Liquid-layering induced, temperature-dependent thermal conductivity enhancement in ZnO-propylene glycol nanofluids. *Chem. Phys. Lett.* **2013**, *561*, 120–124. [CrossRef]
11. Kumar, D.H.; Patel, H.E.; Kumar, V.R.; Sundararajan, T.; Pradeep, T.; Das, S.K. Model for heat conduction in nanofluids. *Phys. Rev. Lett.* **2004**, *93*, 144301. [CrossRef]
12. Nagvenkar, A.P.; Perelshtein, I.; Gedanken, A. Doping effect on the thermal conductivity of metal oxide nanofluids: Insight and mechanistic investigation. *J. Phys. Chem. C* **2017**, *121*, 26551–26557. [CrossRef]
13. Prasher, R.; Bhattacharya, P.; Phelan, P.E. Brownian-motion-based convective-conductive model for the effective thermal conductivity of nanofluids. *J. Heat Mass Transf.* **2006**, *128*, 588–595. [CrossRef]
14. Abbasi, M.; Heyhat, M.; Rajabpour, A. Study of the effects of particle shape and base fluid type on density of nanofluids using ternary mixture formula: A molecular dynamics simulation. *J. Mol. Liq.* **2020**, *305*, 112831. [CrossRef]
15. Selvam, C.; Mohan Lal, D.; Harish, S. Thermal conductivity and specific heat capacity of water-ethylene glycol mixture-based nanofluids with graphene nanoplatelets. *J. Therm. Anal. Calorim.* **2017**, *129*, 947–955. [CrossRef]
16. Hong, J.; Kim, D. Effects of aggregation on the thermal conductivity of alumina/water nanofluids. *Thermochim. Acta* **2012**, *542*, 28–32. [CrossRef]

17. Wu, Z.; Sundén, B. Convective heat transfer performance of aggregate-laden nanofluids. *Int. J. Heat Mass Transf.* **2016**, *93*, 1107–1115. [CrossRef]
18. Motevasel, M.; Nazar, A.R.S.; Jamialahmadi, M. The effect of nanoparticles aggregation on the thermal conductivity of nanofluids at very low concentrations: Experimental and theoretical evaluations. *Heat Mass Transf.* **2018**, *54*, 125–133. [CrossRef]
19. Wensel, J.; Wright, B.; Thomas, D.; Douglas, W.; Mannhalter, B.; Cross, W.; Hong, H.; Kellar, J.; Smith, P.; Roy, W. Enhanced thermal conductivity by aggregation in heat transfer nanofluids containing metal oxide nanoparticles and carbon nanotubes. *Appl. Phys. Lett.* **2008**, *92*, 023110. [CrossRef]
20. Prasher, R.; Phelan, P.E.; Bhattacharya, P. Effect of aggregation kinetics on the thermal conductivity of nanoscale colloidal solutions (nanofluid). *Nano Lett.* **2006**, *6*, 1529–1534. [CrossRef]
21. Pang, C.; Jung, J.Y.; Kang, Y.T. Aggregation based model for heat conduction mechanism in nanofluids. *Int. J. Heat Mass Transf.* **2014**, *72*, 392–399. [CrossRef]
22. Tahmooressi, H.; Kasaeian, A.; Tarokh, A.; Rezaei, R.; Hoorfar, M. Numerical simulation of aggregation effect on nanofluids thermal conductivity using the lattice Boltzmann method. *Int. Commun. Heat Mass Transf.* **2020**, *110*, 104408. [CrossRef]
23. Wang, R.; Qian, S.; Zhang, Z. Investigation of the aggregation morphology of nanoparticle on the thermal conductivity of nanofluid by molecular dynamics simulations. *Int. J. Heat Mass Transf.* **2018**, *127*, 1138–1146. [CrossRef]
24. Li, Y.; Zhai, Y.; Chen, W.; Li, Z.; Wang, H. Microscopic mechanisms of particle agglomeration to enhance transport properties of nanofluids. *J. Mol. Liq.* **2023**, *383*, 122008. [CrossRef]
25. Du, J.; Su, Q.; Li, L.; Wang, R.; Zhu, Z. Evaluation of the influence of aggregation morphology on thermal conductivity of nanofluid by a new MPCD-MD hybrid method. *Int. Commun. Heat Mass Transf.* **2021**, *127*, 105501. [CrossRef]
26. Awad, A.; Navarro, H.; Ding, Y.; Wen, D. Thermal-physical properties of nanoparticle-seeded nitrate molten salts. *Renew. Energy* **2018**, *120*, 275–288. [CrossRef]
27. Anagnostopoulos, A.; Alexiadis, A.; Ding, Y. Molecular dynamics simulation of solar salt ($NaNO_3$-KNO_3) mixtures. *Sol. Energy Mater. Sol. Cells* **2019**, *200*, 109897. [CrossRef]
28. Niégawa, A.; Takashiba, K. Transition rates of reactions in the microcanonical ensemble and the finite-size effect. *Can. J. Phys.* **1993**, *71*, 276–279. [CrossRef]
29. Li, Z.; Cui, L.; Li, B.; Du, X. Enhanced heat conduction in molten salt containing nanoparticles: Insights from molecular dynamics. *Int. J. Heat Mass Transf.* **2020**, *153*, 119578. [CrossRef]
30. Cui, L.; Yu, Q.; Wei, G.; Du, X. Mechanisms for thermal conduction in molten salt-based nanofluid. *Int. J. Heat Mass Transf.* **2022**, *188*, 122648. [CrossRef]
31. Plimpton, S. Fast parallel algorithms for short-range molecular dynamics. *J. Comput. Phys.* **1995**, *117*, 1–19. [CrossRef]
32. Qiao, G.; Alexiadis, A.; Ding, Y. Simulation study of anomalous thermal properties of molten nitrate salt. *Powder Technol.* **2017**, *314*, 660–664. [CrossRef]
33. Qiao, G.; Lasfargues, M.; Alexiadis, A.; Ding, Y. Simulation and experimental study of the specific heat capacity of molten salt based nanofluids. *Appl. Therm. Eng.* **2017**, *111*, 1517–1522. [CrossRef]
34. Janz, G.J.; James, D.W. Raman spectra and ionic interactions in molten nitrates. *J. Chem. Phys.* **1961**, *35*, 739–745. [CrossRef]
35. Hisatsune, I.; Devlin, J.; Califano, S. Urey-Bradley potential constants in nitrogen dioxide, nitrite ion and dinitrogen tetroxide. *Spectrochim. Acta* **1960**, *16*, 450–458. [CrossRef]
36. Aljaerani, H.A.; Samykano, M.; Saidur, R.; Pandey, A.; Kadirgama, K. Nanoparticles as molten salts thermophysical properties enhancer for concentrated solar power: A critical review. *J. Energy Storage* **2021**, *44*, 103280. [CrossRef]
37. Romero, M.; González-Aguilar, J. Solar thermal CSP technology. *Wiley Interdiscip. Rev. Energy Environ.* **2014**, *3*, 42–59. [CrossRef]
38. Lv, W.; Henry, A. Direct calculation of modal contributions to thermal conductivity via Green-Kubo modal analysis. *New J. Phys.* **2016**, *18*, 013028. [CrossRef]
39. Babaei, H.; Keblinski, P.; Khodadadi, J. A proof for insignificant effect of Brownian motion-induced micro-convection on thermal conductivity of nanofluids by utilizing molecular dynamics simulations. *J. Appl. Phys.* **2013**, *113*, 084302. [CrossRef]
40. Li, S.; Guenther, C.L.; Kelley, M.S.; Dixon, D.A. Molecular structures, acid-base properties, and formation of group 6 transition metal hydroxides. *J. Phys. Chem. C* **2011**, *115*, 8072–8103. [CrossRef]
41. Serrano-López, R.; Fradera, J.; Cuesta-López, S. Molten salts database for energy applications. *Chem. Eng. Process. Process Intensif.* **2013**, *73*, 87–102. [CrossRef]
42. Li, Y.; Chen, X.; Wu, Y.; Lu, Y.; Zhi, R.; Wang, X.; Ma, C. Experimental study on the effect of SiO_2 nanoparticle dispersion on the thermophysical properties of binary nitrate molten salt. *Sol. Energy* **2019**, *183*, 776–781. [CrossRef]
43. Nasiri, A.; Shariaty-Niasar, M.; Rashidi, A.M.; Khodafarin, R. Effect of CNT structures on thermal conductivity and stability of nanofluid. *Int. J. Heat Mass Transf.* **2012**, *55*, 1529–1535. [CrossRef]
44. Kazemi-Beydokhti, A.; Heris, S.Z.; Moghadam, N.; Shariati-Niasar, M.; Hamidi, A. Experimental investigation of parameters affecting nanofluid effective thermal conductivity. *Chem. Eng. Commun.* **2014**, *201*, 593–611. [CrossRef]
45. Meibodi, M.E.; Vafaie-Sefti, M.; Rashidi, A.M.; Amrollahi, A.; Tabasi, M.; Kalal, H.S. The role of different parameters on the stability and thermal conductivity of carbon nanotube/water nanofluids. *Int. Commun. Heat Mass Transf.* **2010**, *37*, 319–323. [CrossRef]
46. Zhang, T.; Zou, Q.; Cheng, Z.; Chen, Z.; Liu, Y.; Jiang, Z. Effect of particle concentration on the stability of water-based SiO_2 nanofluid. *Powder Technol.* **2021**, *379*, 457–465. [CrossRef]

47. Chieruzzi, M.; Cerritelli, G.F.; Miliozzi, A.; Kenny, J.M. Effect of nanoparticles on heat capacity of nanofluids based on molten salts as PCM for thermal energy storage. *Nanoscale Res. Lett.* **2013**, *8*, 448. [CrossRef] [PubMed]
48. Shin, D.; Banerjee, D. Enhanced thermal properties of SiO_2 nanocomposite for solar thermal energy storage applications. *Int. J. Heat Mass Transf.* **2015**, *84*, 898–902. [CrossRef]
49. Teng, K.L.; Hsiao, P.Y.; Hung, S.W.; Chieng, C.C.; Liu, M.S.; Lu, M.C. Enhanced thermal conductivity of nanofluids diagnosis by molecular dynamics simulations. *J. Nanosci. Nanotechnol.* **2008**, *8*, 3710–3718. [CrossRef]
50. Eapen, J.; Li, J.; Yip, S. Mechanism of thermal transport in dilute nanocolloids. *Phys. Rev. Lett.* **2007**, *98*, 028302. [CrossRef]
51. Jo, B.; Banerjee, D. Enhanced specific heat capacity of molten salt-based nanomaterials: Effects of nanoparticle dispersion and solvent material. *Acta Mater.* **2014**, *75*, 80–91. [CrossRef]
52. Gorji, T.B.; Ranjbar, A.; Mirzababaei, S. Optical properties of carboxyl functionalized carbon nanotube aqueous nanofluids as direct solar thermal energy absorbers. *Sol. Energy* **2015**, *119*, 332–342. [CrossRef]
53. Fedele, L.; Colla, L.; Bobbo, S.; Barison, S.; Agresti, F. Experimental stability analysis of different water-based nanofluids. *Nanoscale Res. Lett.* **2011**, *6*, 300. [CrossRef] [PubMed]
54. Li, X.; Zhu, D.; Wang, X. Evaluation on dispersion behavior of the aqueous copper nano-suspensions. *J. Colloid Interface Sci.* **2007**, *310*, 456–463. [CrossRef] [PubMed]

Disclaimer/Publisher's Note: The statements, opinions and data contained in all publications are solely those of the individual author(s) and contributor(s) and not of MDPI and/or the editor(s). MDPI and/or the editor(s) disclaim responsibility for any injury to people or property resulting from any ideas, methods, instructions or products referred to in the content.